Cyanide and Nitric Oxide Binding to Reduced Protocatechuate 3,4-Dioxygenase: Insight into the Basis for Order-Dependent Ligand Binding by Intradiol Catecholic Dioxygenases†

Allen M. Orville‡ and John D. Lipscomb*

Department of Biochemistry, Medical School, and Center for Metals in Biocatalysis, University of Minnesota, Minneapolis, Minnesota 55455-0347

Received March 17, 1997; Revised Manuscript Received August 26, 1997⊗

ABSTRACT: EPR-silent, chemically reduced protocatechuate 3,4-dioxygenase (E^r) binds NO at the active site Fe^{2+} to yield an EPR-active, $S = {}^3/_2$ species that blocks subsequent binding of all other exogenous ligands. In contrast, addition of NO to a preformed $E^r{\cdot}CN^-$ complex yields an EPR-active, $S = {}^1/_2$ species [$E^r{\cdot}(CN)_x{\cdot}NO$] that exhibits resolved superhyperfine splitting from $^{13}CN^-$, $^{15/14}NO$, and a protein-derived ^{14}N. Simulations of the EPR spectra observed for the $E^r{\cdot}(CN)_x{\cdot}NO$ complex formed with $^{12}CN^-$ and $^{13}CN^-$ (1:1) show that CN^- binds in two iron ligand sites ($x \geq 2$). The two cyanides exhibit similar, but distinguishable, hyperfine coupling constants. This demonstrates unambiguously that at least three exogenous ligands (two cyanides and NO) can bind to the Fe^{2+} simultaneously and strongly suggests that at least one histidine ligand is retained in the complex. The $E^r{\cdot}(CN)_{\geq 2}{\cdot}NO$ complex readily exchanges both of the bound cyanides for the substrate analog, 2-hydroxyisonicotinic acid *N*-oxide (INO), to form a $E^r{\cdot}INO{\cdot}NO$ complex exhibiting the same $S = {}^3/_2$ type EPR spectrum that is observed for this complex in the absence of CN^-. Because the dead-end $E^r{\cdot}NO$ complex does not accumulate during the exchange, the results suggest that $E^r{\cdot}(CN)_{\geq 2}{\cdot}NO$ and $E^r{\cdot}INO{\cdot}NO$ are in conformational states that allow facile exchange of INO and CN^- but not NO. The results are interpreted in the context of the known X-ray crystal structures for the ferric form of the resting enzyme (E^{ox}) and numerous E^{ox}·substrate, inhibitor, and CN^- complexes, all of which have a charge neutral iron center. It is proposed that the binding of one CN^- causes dissociation of an anionic endogenous ligand which begins a series of conformational changes analogous to those initiated by anionic substrate binding to E^{ox}. This results in a new unique coordination site for NO, and a new second site for CN^-; both cyanide sites are utilized when the enzyme subsequently binds substrates or INO.

Protocatechuate 3,4-dioxygenase (3,4-PCD)[1] is a non-heme Fe^{3+}-containing dioxygenase that catalyzes the cleavage of O_2 concomitant with the opening of the aromatic ring of protocatechuate (3,4-dihydroxybenzoate, PCA) to form β-carboxy-*cis,cis*-muconate. The enzyme has emerged as a prototypical catecholic dioxygenase and has been characterized from greater than 10 widely divergent soil bacteria, although the enzymes isolated from *Pseudomonas putida*,[2] *P. cepacia*, and *Brevibacterium fuscum* have been most extensively investigated [for reviews, see Lipscomb and Orville (1992) and Que and Ho (1996)]. Although the quaternary structures of the enzymes differ, spectroscopic studies showed that they have similar or identical Fe^{3+} ligands [reviewed by Que (1989)]. The specific ligands suggested from these studies were later demonstrated by the crystallographic characterization of 3,4-PCD isolated from *P. putida* (Ohlendorf et al., 1988, 1994). The trigonal bipyramidal coordination sphere of the iron is defined by four protein ligands from the β-subunit.[3] As shown in Scheme 1, inset, Tyr447$^{O\eta}$ and His462$^{N\epsilon 2}$ provide the axial ligands, and Tyr408$^{O\eta}$ and His460$^{N\epsilon 2}$ provide two of the equatorial ligands. Wat827, an exogenous solvent molecule thought to be hydroxide ion (True et al., 1990; Felton et al., 1984), completes the equatorial plane.

Spectroscopic (Lipscomb & Orville, 1992; Whittaker & Lipscomb, 1984a; Orville & Lipscomb, 1989; True et al., 1990) and recent crystallographic (Orville et al., 1997a,b)

† This work was supported by a grant from the National Institute of General Medical Science (GM 24689). A.M.O. acknowledges a NIH predoctoral training grant (GM-07323) and a Doctoral Dissertation Fellowship from the Graduate School, University of Minnesota.

* Correspondence should be addressed to this author at the Department of Biochemistry, 4-225 Millard Hall, University of Minnesota, Minneapolis, MN 55455-0347. E-mail: lipsc001@maroon.tc.umn.edu. Telephone: (612) 625-6454. FAX: (612) 625-2163.

‡ Current address: Institute of Molecular Biology, University of Oregon, Eugene, OR 97403.

⊗ Abstract published in *Advance ACS Abstracts,* October 15, 1997.

[1] Abbreviations: 3,4-PCD, protocatechuate 3,4-dioxygenase; PCA, protocatechuate or 3,4-dihydroxybenzoate; INO, 2-hydroxyisonicotinic acid *N*-oxide; EPR, electron paramagnetic resonance; MOPS, 3-(*N*-morpholino)propanesulfonic acid; TAPS, 3-[[tris(hydroxymethyl)methyl]aminopropanesulfonic acid; E^r, chemically reduced 3,4-PCD; $E^r{\cdot}NO$, nitrosyl species of reduced 3,4-PCD plus NO; $E^r{\cdot}(CN)_x$, reduced 3,4-PCD plus one or more iron-bound cyanide molecules; $E^r{\cdot}(CN)_x{\cdot}NO$, nitrosyl complex formed by addition of NO to a preformed $E^r{\cdot}(CN)_x$ complex; $E^r{\cdot}INO{\cdot}NO$, species obtained either from addition of NO to the $E^r{\cdot}INO$ complex or by addition of INO to the $E^r{\cdot}(CN)_x{\cdot}NO$ complex.

[2] American Type Culture Collection (ATCC) 23975, previously classified as *Pseudomonas aeruginosa.*

[3] The residue numbering is that of *P. putida* and also denotes the subunit chain (Ohlendorf et al., 1994); residues in the α-subunits or β-subunits are numbered from 1 to 200 or from 301 to 538, respectively. Although the amino acid sequence and structure of *B. fuscum* 3,4-PCD are currently not known, all previous spectroscopic results indicate that the iron center in the two enzymes is very similar.

S0006-2960(97)00609-0 CCC: $14.00

Scheme 1: Crystal Structure Determined for the Ferric 3,4-PCD·INO·CN Ternary Complex (Orville et al., 1997b)[a]

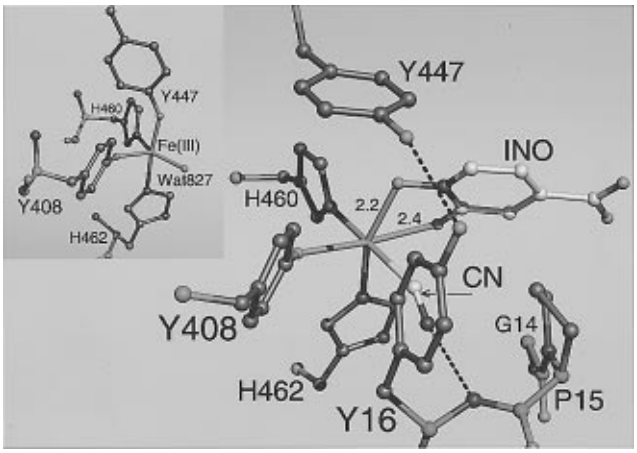

[a] Note the dissociation of Tyr447, the chelation of the substrate analog, the binding of CN^- in the new site created in the iron coordination sphere, and the new pocket created in the protein as a result of conformational change. In the inset, the Fe^{3+} coordination sphere observed in the crystal structure of uncomplexed *P. putida* 3,4-PCD is shown (Ohlendorf et al., 1994). [Prepared with MIDAS+ (Ferrin et al., 1988); from the Computer Graphics Laboratory (supported by NIH Grant RR-01081), University of California, San Francisco.]

studies show that a conformational change in the enzyme structure occurs as a consequence of substrate chelation of the iron. The crystal structures clearly demonstrate (Scheme 1) that substrate chelation (i) displaces the equatorial solvent ligand, (ii) displaces the axial Tyr447, (iii) changes the iron coordination geometry to nearly octahedral, thereby creating a sixth Fe^{3+} coordination site *trans* to $His460^{N\epsilon 2}$, and (iv) creates a small pocket adjacent to both the new sixth coordination site on the iron and the site of ring cleavage on the substrate. The new Fe^{3+} coordination site is unoccupied in the substrate complex. However, our recent crystallographic study of 3,4-PCD complexed with 2-hydroxyisonicotinic acid *N*-oxide (INO, a PCA analog which causes the same structural changes upon binding as PCA) and cyanide (Scheme 1) showed that the latter molecule binds in this site and fills the small cavity created by the structural change (Orville et al., 1997b). These results strongly support the proposal that the new cavity serves to bind O_2 during normal turnover. Interestingly, steric restraints and hydrogen bonding within the O_2 cavity stabilize an unusual Fe^{3+}—C≡N bond that is bent at an angle of approximately 145°. This likely weakens the bond and may explain the failure to observe $^{13}CN^-$ hyperfine interactions with the Fe^{3+} $S = 5/2$ spin system in spectroscopic studies of several ternary enzyme complexes.[4] Although unfavorable for CN^- binding, a bent iron−ligand bond would be favorable for a putative peroxy intermediate which is thought to form after O_2 attack on the substrate (Orville et al., 1997b).

The structures reveal two important contributions of the ligand environment to catalysis. First, PCA binds asymmetrically to the iron. This appears to be due in part to a *trans* ligand influence in which Tyr408 opposite the C3−O^- group of PCA is more electron-supplying than His462 opposite the C4−O^- group which serves to weaken the C3−O−Fe bond. This, in turn, will favor PCA ketonization and localization of charge on C4, thereby promoting electrophilic attack of O_2 on this position. Second, the uncomplexed

[4] A. M. Orville and J. D. Lipscomb, unpublished observations.

Scheme 2: Proposed Structures for the Active Site Metal Center in the (A) E^r·NO and (B) E^r·PCA·NO Complexes[a]

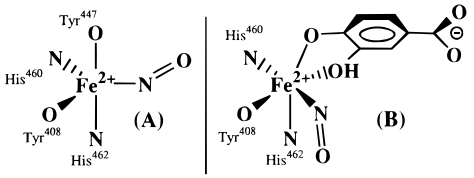

[a] These structures are consistent with the crystal structures of oxidized 3,4-PCD as isolated (Ohlendorf et al., 1994) and the structures of substrate and substrate analog complexes (Orville et al., 1997b).

enzyme, a range of inhibitor complexes, and the substrate or substrate analog complexes are all charge neutral at the iron center. Thus, in the case of PCA association, two anionic ligands (OH^- and $Tyr447^{O\eta}$) are displaced and presumably function to deprotonate the substrate so that it binds as a dianion as required for electrophilic O_2 attack.

Insight into the process of substrate binding that leads from the initial trigonal bipyramidal iron coordination geometry to the eventual octahedral substrate complex has been gained through the crystallographic analysis of several phenolate inhibitor complexes of 3,4-PCD (Orville et al., 1997a). A series of intermediate structures in which substrate first binds weakly to the enzyme, then moves closer to the iron to form a monodentate bond through the ionized C4−O^- group, and finally shifts position to form the dianionic chelate complex and alter the iron coordination geometry is consistent with these structural data.

Another approach to the investigation of the binding process of substrates and small molecules to 3,4-PCD is suggested by our observation that chemically reduced 3,4-PCD ($S = 2$) binds NO to form an EPR-active $S = {}^3/_2$ complex (E^r·NO, Scheme 2A) (Orville & Lipscomb, 1993). Substrates were found to perturb the EPR spectrum of the nitrosyl complex. Moreover, when ^{17}O ($I = {}^5/_2$) was placed specifically in the C4 phenolic hydroxyl group of PCA, superhyperfine coupling was detected, showing that it bound directly to the iron (Scheme 2B). On the other hand, there was no observable hyperfine broadening when the label was placed in the C3−OH group, suggesting that the potential C3−O−Fe^{3+} bond was either weak or absent. This is consistent with the maintenance of charge neutrality at the iron. In contrast, similar experiments using ferric 3,4-PCD in the absence of NO showed that substrate analogs chelate the iron even in the presence of cyanide (Orville & Lipscomb, 1989). Interestingly, a strict order dependence was observed for nitrosyl complex formation with reduced 3,4-PCD. If NO was added first, substrates would not subsequently bind, suggesting that some conformational change must occur upon substrate binding that alters the way in which NO can interact with the enzyme.

Here, our previous approaches are combined in the investigation of the order-dependent binding of NO and CN^- to reduced 3,4-PCD. We find that, when CN^- is the first ligand added, this combination of ligands elicits a rare $S = {}^1/_2$ complex from this non-heme system which gives EPR spectra similar to those of ferrous nitrosyl complexes of hemes. The spectrum is sufficiently well resolved that superhyperfine interactions from several ligands with nonzero nuclear spin are revealed in nearly unprecedented detail to allow determination of many characteristics of the iron ligand composition and geometry. The results are interpreted in the context of the crystal structures of the ferric enzyme

which allows an electronic and structural basis for the observed order dependence to be suggested. The results emphasize the roles of maintenance of charge neutrality at the metal center, *trans* ligand influence, and conformational change in controlling ligation of the iron center. These aspects of the 3,4-PCD active site structure have direct relevance to catalysis of the active ferric form of the enzyme and may also have significance for metalloenzyme catalysis in general.

EXPERIMENTAL PROCEDURES

Chemicals. Potassium cyanide enriched to 99 atom % in either ^{13}C or ^{15}N was obtained from MSD Isotopes. ^{15}NO enriched to 99 atom % ^{15}N was obtained from ICON and used without further purification. ^{14}NO was obtained from Matheson Gas Products (Chicago, IL) and passed over solid NaOH immediately before use. ^{57}Fe enriched to approximately 95 atom % was obtained either as an oxide from Oak Ridge National Laboratory or in elemental form from U. S. Services Inc. (Summit, NJ) and used in bacterial growth media as previously reported (Whittaker et al., 1984). Water enriched to approximately 50 atom % ^{17}O was obtained from Mound Laboratory or ICON. The water was distilled twice in a microdistillation apparatus before use [see Whittaker and Lipscomb (1984a) and Arciero et al. (1985)]. Sample prepared with ^{17}O-enriched water was as described earlier (Orville & Lipscomb, 1993). 2-Hydroxyisonicotinic acid *N*-oxide (INO) was synthesized as previously described (Whittaker & Lipscomb, 1984b).

Enzyme Purification and Assays. The 3,4-PCD was purified from either *P. putida* or *B. fuscum* as previously described (Que et al., 1976; Whittaker et al., 1984, 1990). Experiments with the enzyme isolated from *P. putida* were at pH 8.4 in 50−300 mM Tris buffer. Studies with the 3,4-PCD isolated from *B. fuscum* were at either pH 7.0 in 50−300 mM MOPS buffer or pH 8.4 in 50−300 TAPS buffer. Dioxygenase activity was routinely assayed by measuring the oxygen uptake with a Clark-type oxygen electrode (Whittaker et al., 1990).

Anaerobic Procedures and Nitric Oxide Addition. Enzyme samples[5] were made anaerobic by repeated cycles of evacuation and flushing with argon that had been passed over a column of BASF Inc. copper catalyst at 170 °C to remove residual oxygen. Reduced enzyme samples were prepared as described earlier (Orville & Lipscomb, 1993). Anaerobic reduced enzyme was prepared in a serum-stoppered vial and then transferred with a gas-tight syringe to the EPR tube under argon. Nitric oxide was added by slowly bubbling NO gas through the solution in the EPR tube for approximately 10 min. An argon flow was maintained above the sample to remove excess NO and protect the sample from O_2. Samples were frozen by immersion in liquid N_2. Nitric oxide is highly toxic, and all procedures were conducted in a ventilated hood.

For experiments in which the NO was added before the cyanide or organic ligand, a customized reaction chamber was used as described previously (Orville & Lipscomb, 1993). The reduced enzyme solution was allowed to equilibrate in a NO atmosphere for 10−30 min under reduced light. The cyanide was then added and, after 5−60 min of stirring, the sample was transferred to the EPR tube and frozen by slow immersion into a dry ice/2-propanol bath. The excess NO atmosphere above the sample was eliminated by evacuation and replaced with Ar.

Preparation of Reduced 3,4-PCD·Cyanide·NO Complex. Stock solutions of anaerobic 1−2 M cyanide were prepared by degassing solid NaCN or KCN in a serum-stoppered reaction vial. Anaerobic 1 M buffer (MOPS at pH 7.0, or TAPS at pH 8.4, or Tris at pH 8.4) was added with a gas-tight syringe; the pH was adjusted with the slow addition of anaerobic 8 N H_2SO_4 and verified with pH paper. The enzyme was reduced with 10−20 mM sodium dithionite, the cyanide was added anaerobically to 10−300 mM final concentration, and then the solution was transferred anaerobically to the EPR tube. ^{14}NO was added to the sample through a 28 gauge stainless-steel needle. Bubbles from 200−300 μL of NO were allowed to mix through the solution for 5−10 min by repeated inversions of the EPR tube and then eliminated from the tube with a stream of purified Ar. The ^{15}NO (200 μL) was added in a similar order but from a gas-tight syringe equipped with a valved needle to allow transfer of the ^{15}NO to the sample with the syringe. After the solution was transferred to the anaerobic EPR tube, it was frozen with a dry ice/2-propanol bath. The syringe needle, after piercing the septum closure at the top of the EPR tube, was evacuated and flushed with Ar. After the reduced enzyme−cyanide solution was thawed, the valved syringe was opened, and the gas was added to the solution. The small bubbles of ^{15}NO were mixed with the solution and then eliminated from the tube as above.

Nitric Oxide Photodissociation. Nitric oxide was photodissociated from frozen samples of $E^r\cdot(CN)_x\cdot NO$ complex at 2−20 K in the EPR cryostat by irradiation with white light from a 300 W quartz halogen lamp as previously described (Orville & Lipscomb, 1993; Orville et al., 1992). Photodissociation of NO at 10 °C was performed with a 500 W projection bulb after the enzyme sample was thawed anaerobically and sealed under either an Ar or an NO atmosphere in the EPR tube. The sample was suspended in a circulating temperature-controlled water bath during photolysis.

EPR Spectroscopy. EPR spectra were recorded at X-band with a Varian E-109 spectrometer equipped with an Oxford Instruments ESR-910 liquid helium cryostat. Temperature and *g*-value calibrations were as previously described (Arciero et al., 1983; Whittaker et al., 1984). Data were recorded for integration and subtraction procedures with a digital computer interfaced directly to the spectrometer. Spin quantitations were performed by double integration of the first-derivative spectra by the method of Aasa and Vänngård (1975). EPR spectra of spin $S = {}^3/_2$ complexes were analyzed according to the spin Hamiltonian:

$$\hat{H}_e = \hat{H}_{Zeeman} + \hat{H}_{zero-field} + \hat{H}_{hyperfine} \quad (1)$$

$$\hat{H}_e = g_o\beta_e\vec{S}\cdot\vec{H} + D\left[\hat{S}_z^2 - \frac{5}{4} + \frac{E}{D}(\hat{S}_x^2 - \hat{S}_y^2)\right] + \vec{I}_L\cdot\tilde{A}_L\cdot\vec{S} + \vec{I}_{Fe}\cdot\tilde{A}_{Fe}\cdot\vec{S} \quad (2)$$

where *D* and *E/D* are zero-field splitting parameters and the other terms have the usual definition. EPR spectra of low-spin $S = {}^1/_2$ complexes were analyzed according to the spin

[5] The studies described here were performed with enzyme isolated from *B. fuscum* (ATCC 15993) and *P. putida* (ATCC 23975). The results in all cases were very similar; consequently, the somewhat more highly resolved data from the enzyme from *B. fuscum* are presented except where noted.

Hamiltonian:

$$\hat{H}_e = \beta_e \vec{S}\cdot\tilde{g}\cdot\vec{H} + \vec{I}_L\cdot\tilde{A}_L\cdot\vec{S} + \vec{I}_{Fe}\cdot\tilde{A}_{Fe}\cdot\vec{S} \qquad (3)$$

In eqs 2 and 3, $\tilde{A}_L$ and $\tilde{A}_{Fe}$ are the transferred hyperfine coupling tensors of the ligand or iron, respectively. The hyperfine terms $\vec{I}_L\cdot\tilde{A}_L\cdot\vec{S}$ and $\vec{I}_{Fe}\cdot\tilde{A}_{Fe}\cdot\vec{S}$ describe the interaction of the unpaired electron spin with the nuclear spin of the ligand or metal center, respectively.

Simulations of the $S = {}^1/_2$ EPR Spectral Line Shape. Numerical simulations of the $S = {}^1/_2$ complexes were performed using the FORTRAN program "EPRGHA", in which the hyperfine terms are treated by perturbation theory, retaining only the component diagonal with the electronic Zeeman interaction. This causes a negligible error for small hyperfine splittings such as those encountered here. The program, obtained from Dr. E. Münck, allows input for *g*-values, line widths, and hyperfine coupling constants for up to four nuclei. A Gaussian line shape was utilized; no attempt to improve the fits of the simulated spectra by calculating a Lorentzian line shape was made. No further attempt has been made to improve the EPR line shape simulations by rotating the orientation of the hyperfine coupling tensor relative to the *g*-tensor (LoBrutto et al., 1983). Once the hyperfine splitting pattern was adequately modeled from the $E^r\cdot(^{12}CN)_x\cdot{}^{15}NO$ low-spin complex, the spectrum from the $E^r\cdot(^{13}CN)_x\cdot{}^{15}NO$ (^{13}C, $I = {}^1/_2$) complex was simulated by incorporation of either one or two coupling constants (see text) for the ^{13}C nucleus into the simulation parameter set without making other changes. Simulations for complexes containing ^{14}NO were made using the coupling constant determined for ^{15}NO divided by 1.403, the ratio of the nuclear *g*-values of ^{15}N and ^{14}N (Bolton, 1972). The EPR line shape for the ^{57}Fe-enriched $E^r\cdot(^{12}CN)_x\cdot{}^{15}NO$ complex was simulated with one species of iron by adding the coupling from the ^{57}Fe ($I = {}^1/_2$) nucleus to the parameters from the $[^{56}Fe]$-$E^r\cdot(^{12}CN)_x\cdot{}^{15}NO$ sample.

RESULTS

EPR Spectra of Reduced 3,4-PCD Nitrosyl Complexes. Previous studies have shown that formation of the nitrosyl complexes of E^r or E^r·PCA elicits different $S = {}^3/_2$ EPR spectra depending on the order of addition of the ligands (Orville & Lipscomb, 1993). [The combination of E^r+NO+PCA gives a spectrum with $E/D = 0.055$, which is indistinguishable from that of the E^r·NO complex, while E^r+PCA+NO yields a spectrum with $E/D = 0.175$ (Orville & Lipscomb, 1993).] Similarly, addition of CN^- to a preformed E^r·NO complex does not alter the $S = {}^3/_2$ EPR spectrum ($E/D = 0.055$, Figure 1A). However, the addition of NO to a preformed reduced 3,4-PCD·cyanide complex $[E^r\cdot(CN)_x]$ at pH 7.0−8.5 yields a species $[E^r\cdot(CN)_x\cdot NO]$ with an intense EPR signal and *g*-values at 2.05, 2.00, and 1.95 (Figure 1B). This signal is characteristic of an $S = {}^1/_2$ system and represents one of the few low-spin, non-heme systems known. The dramatic alteration of the spin state suggests that both exogenous ligands bind to iron simultaneously in the $E^r\cdot(CN)_x\cdot NO$ complex. This is demonstrated directly by the observation of nuclear hyperfine splitting in the $S = {}^1/_2$ EPR spectrum as shown below.

Addition of the tight binding "transition state" analog, INO ($K_{D\ overall} = 0.06\ \mu M$; Whittaker & Lipscomb, 1984a), to a preformed $E^r\cdot(CN)_x\cdot NO$ complex causes a rapid loss of the $S = {}^1/_2$ signal and formation of two $S = {}^3/_2$ species (~80% $E/D = 0.048$, ~20% $E/D = 0.170$, Figure 1C). This spectrum is identical to that previously observed for the $E^r\cdot$-INO·NO complex (Orville & Lipscomb, 1993), suggesting that INO displaces the cyanide but not NO from the complex. If during the exchange process an intermediate $E^r\cdot NO$ complex formed with the same characteristics as the species formed by mixing E^r and NO, no binding of INO would be expected due to the strict order dependence described above. This suggests that the prebinding of CN^- causes a change in the way NO binds and that the resulting complex has a long lifetime relative to the rate of ligand exchange.

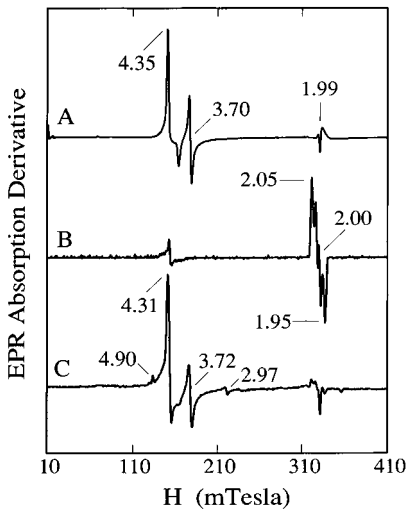

FIGURE 1: Different EPR-active species are obtained depending upon the order of addition of NaCN, NO, or INO to reduced 3,4-PCD. (A) 3,4-PCD (60 μM) in 200 mM MOPS buffer at pH 7.0 was reduced with 20 mM sodium dithionite and exposed to NO followed by the addition of ~180 mM NaCN. The integrated intensity of the $S = {}^3/_2$ species was observed to account for >95% of the iron present in the sample before addition of NaCN. (B) 3,4-PCD (~37 μM) in 100 mM Tris buffer, pH 8.0, was reduced with 20 mM sodium dithionite, incubated with 100 mM [^{13}C]KCN for 5 min, and subsequently exposed to ^{15}NO at 5 °C. (C) Sample from (B) was thawed anaerobically under reduced light, and 9.4 mM INO was added, mixed, and frozen within 1 min. Instrumental conditions: for (A and C) temperature = 5 K, microwave power = 0.2 mW, microwave frequency = 9.2 GHz, modulation amplitude = 1 mT, modulation frequency = 100 kHz; for (B) same as (A and C) except for temperature = 15 K, modulation amplitude = 0.1 mT, microwave power = 0.04 mW.

Despite the apparent high affinity of NO for the ferrous center in E^r, double integration of the $S = {}^1/_2$ EPR spectrum from several $E^r\cdot(CN)_x\cdot NO$ complexes reveals variable amounts of $S = {}^1/_2$ species that roughly correlate with sample incubation times. Under the conditions outlined under Experimental Procedures, the $S = {}^1/_2$ species typically accounts for approximately 50% of the iron in the sample. Typically, no other EPR resonances are observed (except for a very small resonance at $g = 4.3$ derived from oxidized enzyme), showing that all the iron is present in either the $S = {}^1/_2$ or the EPR-silent species.[6] Accordingly, the Mössbauer spectrum (data not shown) of the ^{57}Fe-enriched $E^r\cdot(CN)_x\cdot$-NO complex frozen rapidly after generation of the complex revealed the presence of both $S = {}^1/_2$ and $S = 0$ spin systems in an approximately 1:1 ratio. After a 1 h incubation of the $E^r\cdot(CN)_x\cdot NO$ complex at 5−10 °C, all of the EPR-active species were lost, and a commensurate increase in the $S = 0$ species detected by Mössbauer spectroscopy was observed. Subsequent additional exposure of these samples to NO does not elicit any EPR-detectable species, suggesting that CN^- binding is capable of excluding NO after the final low-spin

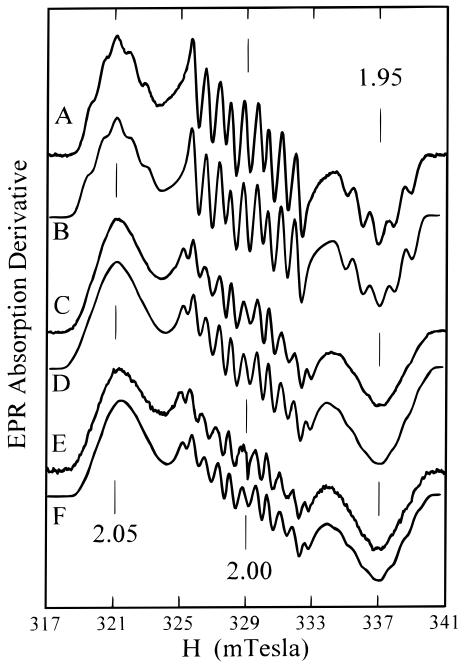

FIGURE 2: EPR spectra of the low-spin $E^r\cdot(CN)_x\cdot NO$ complex formed with ^{14}NO. Approximately 70 μM *B. fuscum* 3,4-PCD was reduced with 20 mM dithionite in anaerobic 200 mM TAPS buffer (pH 8.4) and mixed with either (A)100 mM [^{12}C]NaCN or (*C*) [^{13}C]KCN followed by addition of ^{14}NO. (E) For comparison, the spectrum is shown of *P. putida* 3,4-PCD (~50 μM) in 200 mM Tris buffer (pH 8.4) reduced with 20 mM dithionite and mixed with 100 mM [^{13}C]KCN followed by addition of ^{14}NO. Numerical simulations of $S = {}^1/_2$ EPR line shapes (B, D, and F) are based on the presence of two cyanide ligands (model 2) and the parameters given in Table 1. The experimental spectra shown are the sum of 10 spectra. The instrumental conditions were as follows: 25 mT sweep width; field center, 329 mT; scan rate, 3.1 mT/min; microwave power, 0.04 mW; microwave frequency, 9.2 GHz; modulation frequency, 100 kHz; modulation amplitude, 0.1 mT; temperature, 20 K.

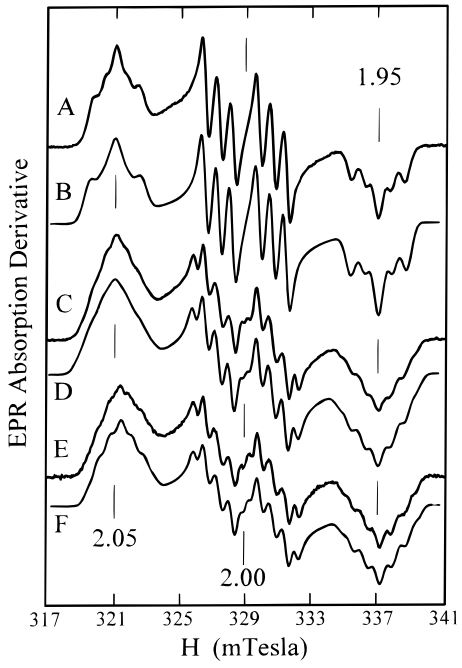

FIGURE 3: EPR spectra of the low-spin $E^r\cdot(CN)_x\cdot NO$ complex formed with ^{15}NO. Approximately 70 μM 3,4-PCD was reduced with 20 mM dithionite in anaerobic 200 mM TAPS buffer (pH 8.4). The cyanide and NO were added as described under Experimental Procedures and spectra collected as in Figure 2. Reduced enzyme was mixed with (A) 100 mM [^{12}C]NaCN (*B. fuscum* 3,4-PCD), (C) 100 mM [^{13}C]KCN (*B. fuscum* 3,4-PCD), or (E) 100 mM [^{13}C]KCN *(P. putida* 3,4-PCD) followed by addition of ^{15}NO. Numerical simulations of the $S = {}^1/_2$ EPR line shape (B, D, and F) are based on the presence of two cyanide ligands (model 2) and the parameters given in Table 1.

$S = 0$ species is formed. By analogy with cyanide addition to the Fe^{3+} enzyme, this final species probably represents two or three CN^- bound simultaneously to the iron (Orville & Lipscomb, 1989).

Nuclear Hyperfine Splitting in the $S = {}^1/_2$ EPR Spectra. As shown in Figures 2 and 3, the $E^r\cdot(CN)_x\cdot NO$ complex yields a well-resolved, maximally rhombic EPR spectrum symmetric about $g = 2.00$.[5] The EPR spectrum of this nonheme iron complex strongly resembles those observed for ferrous nitrosyl heme complexes [see, for example, Kon and Katoaka (1969), Yonetani et al. (1972), and Stevens and Chan (1981)]. However, the EPR spectra from heme $Fe^{2+}\cdot NO$ complexes are generally more axial and the hyperfine splitting in the high- and low-field resonances is much less well resolved than in the spectrum from the $E^r\cdot(CN)_x\cdot NO$ complex reported here. The $g = 2.00$ resonance in the EPR spectrum of the $E^r\cdot(^{12}C^{14}N)_x\cdot{}^{14}NO$ complex is split into a nine-line pattern, probably resulting from a triplet of triplets (Figure 2A). Such a pattern would be obtained from the hyperfine coupling of two inequivalent, $I = 1$ nuclei to the electronic spin of the $Fe^{2+}\cdot NO$ center. Indeed, two $I = 1$ nuclear hyperfine splitting constants of approximately 23 and 8 G are observed. The EPR spectra from heme $Fe^{2+}\cdot NO$ complexes exhibit nearly the same magnitude hyperfine splittings which have been shown to arise from the exogenous nitrosyl nitrogen and the nitrogen of the axial histidine ligand, respectively (Stevens & Chan, 1981).

Formation of the $E^r\cdot(^{12}C^{14}N)_x\cdot{}^{15}NO$ complex (^{15}N, $I = {}^1/_2$) yields a central resonance with a resolved doublet of triplets (Figure 3A) with splitting constants of approximately 32 and 8 G, respectively. The increase in the hyperfine splitting constant by a factor of approximately 1.4 upon substitution of ^{15}NO for ^{14}NO is very close to that expected. Since only the larger hyperfine splitting is dependent on the isotope of NO used, it derives from the nitrogen atom of NO, while the smaller splitting derives from an $I = 1$ atom common to both the $E^r\cdot(^{12}C^{14}N)_x\cdot{}^{14}NO$ and $E^r\cdot(^{12}C^{14}N)_x\cdot{}^{15}NO$ complexes. The $E^r\cdot(^{12}C^{15}N)_x\cdot{}^{14}NO$ complex yields a hyperfine splitting pattern identical to the $E^r\cdot(^{12}C^{14}N)_x\cdot{}^{14}NO$ complex (data not shown), and, therefore, the smaller triplet is not due to the [^{14}N]cyanide atom. Consequently, the $I = 1$ triplet is very likely to originate from one (or both) [^{14}N]$His^{N\epsilon 2}$ ligand(s) known to coordinate the iron from crystal structures of the oxidized enzyme and numerous ligand complexes (Ohlendorf et al., 1988, 1994; Orville et al., 1997a,b).

Direct coordination of the cyanide to the Fe^{2+} of the $E^r\cdot(CN)_x\cdot NO$ complex is clearly established by the altered hyperfine splitting pattern observed when the complex is formed with [^{13}C]cyanide ($I = {}^1/_2$) (Figures 2C and 3C). Each resonance, and especially the $g = 2.00$ signal, exhibits additional features relative to the [^{12}C]cyanide complexes. Formation of the $E^r\cdot(CN)_x\cdot NO$ complex with enzyme containing ^{57}Fe ($I = {}^1/_2$) also yields an altered hyperfine splitting pattern (Figure 4A). Together, the EPR spectral perturba-

[6] Occasionally, prolonged incubation of reduced 3,4-PCD with NO (or CN^- and NO) elicits an EPR signal from an integer spin system. In a parallel mode EPR cavity, these resonances have a *g*-value between 8 and 9, suggesting an $S = 2$ spin state (Orville, Hendrich, and Lipscomb, unpublished observations). The origin of this species is currently under further investigation.

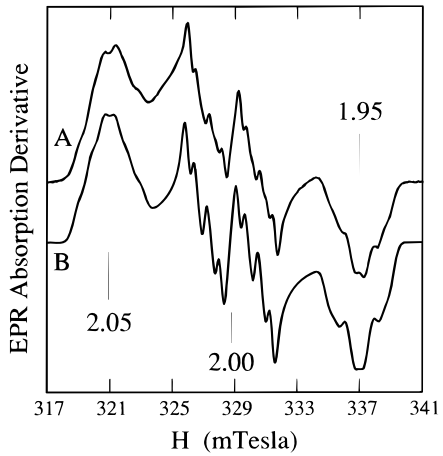

FIGURE 4: EPR spectra of the low-spin ^{57}Fe-enriched E^r·(^{12}CN)$_x$·^{15}NO complex. 3,4-PCD (400 μM) in MOPS buffer at pH 7.0 was reduced with approximately 50 mM dithionite and incubated with 175 mM [^{12}C]NaCN followed by 10 min exposure to ^{15}NO (A). Data collection and instrumental conditions are as in Figure 2. Numerical simulation of the EPR line shape (B) using the parameters listed in Table 1 suggests that the entire population of iron exhibits approximately the same magnitude of hyperfine splitting by the ^{57}Fe nucleus.

tions caused by isotopic substitutions demonstrate that the ferrous center coordinates NO, at least one CN^-, and at least one His ligand. The nuclear hyperfine splitting pattern does not change when the E^r·(CN)$_x$·NO complex is formed with enzyme rehydrated in ^{17}O-enriched water, suggesting that solvent is not an iron ligand (data not shown). The pattern is also unaffected by changes in pH between 7.0 and 8.4 as well as the addition of substrates and inhibitors such as PCA and 4-OH-benzoate. The hyperfine splitting pattern does not change between temperatures of 2 and 40 K or in the microwave power range between 40 μW and saturation (>0.2 mW), suggesting that there are no additional EPR-active species.

Numerical Simulations of the $S = {}^1/_2$ EPR Spectral Line Shape. The EPR spectrum from the E^r·(CN)$_x$·NO complex can be simulated as described under Experimental Procedures in order to characterize and quantitate the nuclear hyperfine interactions. To a first approximation, a reasonably good fit to the $g = 2.00$ resonance in the E^r·(^{12}CN)$_x$·^{15}NO complex (Figure 3A) is obtained from the hyperfine splitting pattern shown in Figure 5B and Table 1. Estimating the coupling constant of [^{13}C]cyanide in the splitting pattern from the E^r·(^{13}CN)$_x$·^{15}NO complex is more difficult because the resonance is only partially resolved as shown in the expanded spectrum in Figure 5D. Surprisingly, the addition of coupling from an $I = {}^1/_2$ nucleus (Figure 5A) of sufficient magnitude to match the outer features of the $g = 2.00$ resonance (Figure 5D) does not yield a satisfactory fit of the ^{13}C nuclear hyperfine splitting pattern. Additional attempts to model this spectral line shape with coupling from three nuclei (^{15}NO, and two [^{14}N]His) or four coupling nuclei (^{15}NO, ^{13}CN, and two [^{14}N]His) also proved unsuccessful (data not shown). It is unlikely that this pattern results from the presence of two significantly different forms of the enzyme because essentially the same pattern is observed from both the *B. fuscum* (Figures 2C and 3C) and the *P. putida* (Figures 2E and 3E) enzymes. Also the spectrum of the ^{57}Fe-containing sample was modeled well as a single species, suggesting that there is only a single type of iron environment (Figure 4, Table 1). The spectrum can be adequately simulated by either of two models involving a single form

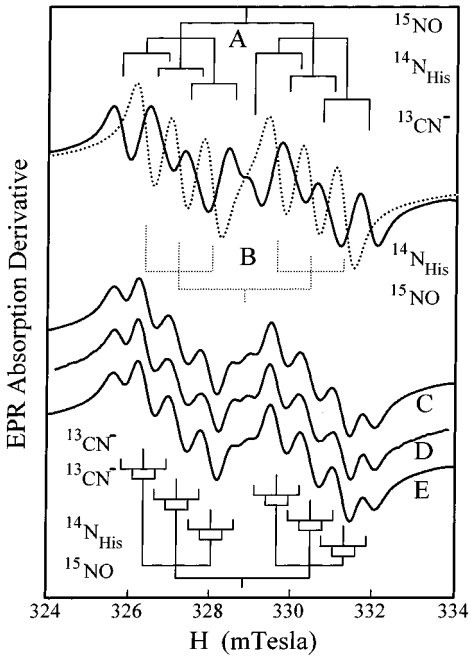

FIGURE 5: Numerical simulation of the g = 2.001 EPR line shape from the E^r·(^{13}CN)$_x$·^{15}NO complex suggests two possible cyanide binding models. For the model in which cyanide can bind and couple strongly to the electronic spin in only one of two binding sites (model 1), one species exhibits large ^{13}C hyperfine coupling (A) and the other does not (B). When the two species are summed (0.45 A plus 0.55 B), the EPR line shape (C) very closely approximates the experimental line shape (D). For the model in which two cyanide ligands bind simultaneously to the iron and exhibit similar coupling constants (model 2), the simulated spectrum (E) also matches the experimental spectrum quite well using the parameters given in Table 1.

of the enzyme. In model 1, it is assumed that: (a) two $S = {}^1/_2$ species are present in roughly equal concentrations due to CN^- binding in either of two Fe^{2+} ligands sites; (b) in one species, the ^{13}C nuclear spin couples strongly (Figure 5A) while no ^{13}C coupling is observed in the other (Figure 5B); and (c) the coupling constants for all other nonzero spin nuclei are identical in the two species. In model 2, it is assumed that two cyanides are always bound in two ligand sites and that they exhibit similar hyperfine coupling constants that are about half that for the strongly coupled CN^- described in model 1. Simulations show that both model 1 (Figure 5C) and model 2 (Figure 5E) reproduce every aspect of the observed EPR spectral line shape (Figure 5D) for the exogenous ligand isotopic substitutions. The resolution of the spectrum and the simulations is adequate to state either that (a) the two sites are not precisely equally occupied (in model 1) or that (b) the two cyanides have slightly different coupling constants (in model 2) (see Figure 5 and Table 1).

The question of whether model 1 or model 2 applies to the E^r·(CN)$_x$·NO complex can be explored by forming the complex with a 1:1 mixture of $^{12}CN^-$ and $^{13}CN^-$ shown in Figure 6C. As shown in Figure 6A,B, simulations of the expected spectra under the assumptions of models 1 and 2, respectively, lead to quite different resultant spectra. The observed spectrum is much more similar to that predicted for model 2, strongly suggesting that two cyanides with similar, but distinguishable, coupling constants are bound to the active site Fe^{2+} simultaneously with NO (i.e., $x \geq 2$).

The set of nuclear hyperfine splitting constants determined for the ^{15}NO complexes can be used to predict the splitting

Table 1: Nuclear Coupling Constants (A) in the E^r·$(CN)_x$·NO Complex[a]

g-value	nucleus	*B. fuscum*[b] (MHz)	*P. putida*[c] (MHz)
2.050	^{15}NO	4.190	4.10
	^{14}NO	2.960	2.960
	$^{13}CN^-$ [d]	3.210	3.330
	$^{13}CN^-$ [e]	1.685; 1.685	1.595; 1.515
	^{14}N-enzyme	2.30	2.00
	^{57}Fe-enzyme	2.20	ND[f]
2.00	^{15}NO	9.10	9.10
	^{14}NO	6.380	6.380
	$^{13}CN^-$ [d]	3.190	3.190
	$^{13}CN^-$ [e]	1.675; 1.595	1.595; 1.515
	^{14}N-enzyme	2.30	2.30
	^{57}Fe-enzyme	1.380	ND
1.950	^{15}NO	4.50	4.250
	^{14}NO	3.140	2.980
	$^{13}CN^-$ [d]	3.190	3.190
	$^{13}CN^-$ [e]	1.675; 1.675	1.675; 1.595
	^{14}N-enzyme	2.30	2.30
	^{57}Fe-enzyme	1.40	ND

[a] The hyperfine coupling constants (A) used in the simulations of this report were converted from the observed hyperfine splitting (a) by the following relationship: $a = hA/\beta g$, where $h/\beta = 0.7144$. [b] Line shape simulations were performed with the following variables (g-value and line width): $g_1 = 2.050$, 0.85 mT; $g_2 = 2.0010$, 0.45 mT; $g_3 = 1.9535$, 0.70 mT; microwave frequency, 9.2158 GHz; Gaussian line shape. [c] Line shape simulations were performed with the following variables (g-value and line width): $g_1 = 2.0480$, 0.66 mT; $g_2 = 2.0012$, 0.45 mT; $g_3 = 1.9533$, 0.64 mT; microwave frequency, 9.2182 GHz; Gaussian line shape. [d] Model 1 (see Figure 5C): a CN^- ligand in either of two sites in which 0.45 of the $S = {}^1/_2$ EPR active species demonstrates ^{13}C hyperfine coupling (Figure 5A) and the other 0.55 fraction does not exhibit coupling (Figure 5B). [e] Model 2 (see Figure 5E): two CN^- ligands that demonstrate ^{13}C hyperfine coupling. [f] Not determined.

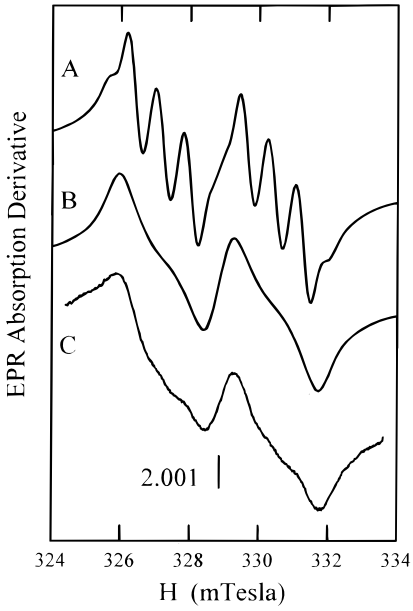

FIGURE 6: Simulated and observed line shapes for cyanide binding models 1 and 2 when the E^r·$(CN)_x$·^{15}NO complex is formed with equimolar $^{12}CN^-$ and $^{13}CN^-$. (A) Simulation for model 1 based on the summation of the 50% spectrum with no ^{13}C coupling and 50% of the spectrum shown in Figure 5C. (B) Simulation for model 2 based on the statistical distribution for $^{13}CN^-$ and $^{12}CN^-$ binding in two sites randomly. The ^{13}C hyperfine coupling constants shown in Table 1 were used for the $^{13}CN^-$ binding in the two slightly inequivalent sites as revealed by the simulation of the spectrum shown in Figure 5D. (C) The E^r·$(CN)_x$·^{15}NO complex was formed as described in Figure 3C except that the cyanide used was an equimolar mixture of $^{12}CN^-$ and $^{13}CN^-$.

pattern after ^{14}NO isotopic substitution by scaling the NO hyperfine splitting constant by the ratio of ^{14}N to ^{15}N nuclear g-values. This yields excellent simulations of the EPR spectral line shape for each complex formed with ^{14}NO (Figure 2B,D,F) *without* further adjustment. Therefore, this simulation strategy produces a set of self-consistent nuclear hyperfine splitting constants for all isotopic substitutions in this report.

Estimation of the magnitude of the nuclear hyperfine splitting constants for the $g = 1.95$ and 2.05 resonances is, in principle, more difficult because the splitting patterns are not as well resolved as for the $g = 2.00$ resonance. However, requiring self-consistent hyperfine splitting constants for all combinations of isotopically substituted ligands yields very good estimates for all the nuclear hyperfine coupling constants in the $g = 2.05$ and 1.95 resonances (Figures 2−4; Table 1).

Several concluding observations regarding the hyperfine coupling constants determined from these simulations can be made (Table 1): (i) The magnitudes of the coupling constants in the $g = 2.00$ resonance for NO and [^{14}N]His are very similar to those observed for many of the nitrosyl heme complexes. (ii) The E^r·$(CN)_{\geq 2}$·NO complex formed with enzyme isolated from either *B. fuscum* or *P. putida* 3,4-PCD yields nearly identical hyperfine coupling constants (Table 1; Figures 2 and 3). (iii) The coupling constant for [^{14}N]His is the same in all three resonances. (iv) Similarly, isotropic coupling of the ^{13}C nucleus of cyanide is observed. (v) In contrast, anisotropic hyperfine splitting from the ^{57}Fe nucleus and ^{14}NO or ^{15}NO is observed.

Photolysis of the Fe^{2+}−NO Bond Promotes Isotopic NO Exchange. Exposure of the E^r·$(CN)_{\geq 2}$·NO complex to white light at 5−20 K in the EPR cryostat results in rapid loss of the $S = {}^1/_2$ EPR spectral intensity (Figure 7, inset). Although the extent of decrease in the EPR signal intensity is dependent upon sample temperature and the intensity of the incident light, the line shape of the residual EPR spectrum is indistinguishable from that of the E^r·$(CN)_{\geq 2}$·NO complex before illumination. This suggests that there is no change in the ligand set responsible for the residual $S = {}^1/_2$ spectrum. When the light is extinguished, the EPR spectral intensity returns to the original level over several hours at 2−20 K. However, the full intensity of the spectrum can be restored rapidly by a brief temperature excursion to 80 K within the EPR cryostat. These observations are consistent with photodissociation and subsequent geminate recombination of the NO molecule. Although CN^- might also be dissociated (Mitchel et al., 1995), the complete loss of the EPR spectrum for a large fraction of the enzyme population and the lack of alterations to the hyperfine splitting pattern or spin state are more consistent with NO photodissociation. Moreover, no $S = {}^3/_2$ EPR spectrum is observed during the process as might be expected if CN^- dissociated.

The highly resolved EPR spectral features of the E^r·$(CN)_{\geq 2}$·NO complex are ideal for examining aspects of NO photodissociation, geminate recombination, and ligand exchange for the reduced enzyme. A preformed E^r·$(^{12}CN)_{\geq 2}$·^{14}NO complex that is subsequently *re-equilibrated in the dark* in solution with ^{15}NO has the potential for isotopic exchange of the NO either upon "re-equilibration" or upon recombination after photolysis of the Fe^{2+}—NO bond. As shown in Figure 7A, this sample exhibits the hyperfine splitting pattern characteristic of ^{14}NO, demonstrating that exchange with ^{15}NO in solution does not occur in the dark at 5−10 °C during the 10 min incubation period. Repeated photodis-

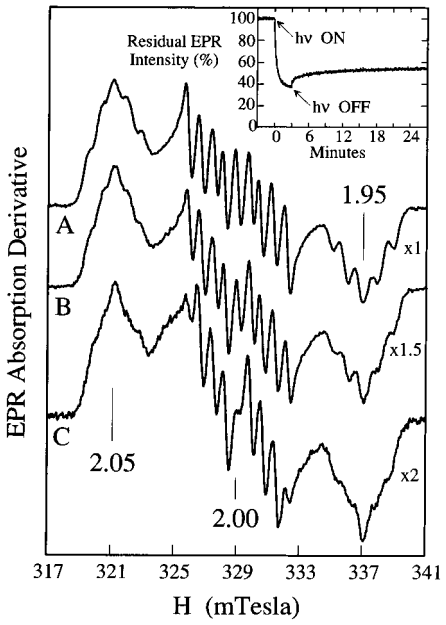

FIGURE 7: $^{14}NO-^{15}NO$ exchange in the $S = {}^1/_2$ complex is possible by photodissociation of the NO, but only in solution. Reduced 3,4-PCD was incubated first with $^{12}CN^-$ and then ^{14}NO (A). The sample from (A) was thawed anaerobically in subdued light, and the solution was equilibrated with ^{15}NO for 10 min. Inset: loss of EPR intensity of at $g = 2.05$ (field set at 321 mT) by photodissociation at 20 K in the EPR cryostat. At time zero, the light was turned on (arrow) and extinguished after 3 min, and the rebinding rate was observed. Incubation of the sample at 77 K allowed complete recovery of the EPR intensity. As shown in (B), only ^{14}NO rebinds at temperatures between 20 and 77 K. The sample from (B) was then thawed anaerobically, illuminated at 0 °C for 10 min with a 500 W projector, and frozen, and the EPR line shape was recorded (C). The loss of total EPR intensity in the EPR spectra from (A) to (C) is probably the result of CN^- displacing the NO from its binding site, yielding an increasing amount of $S = 0$ species that is EPR-silent. Data collection and instrumental conditions are as in Figure 2.

sociation and recombination of this "re-equilibrated" sample at 4−230 K yield an unaltered hyperfine pattern (Figure 7B). This suggests that isotopic exchange with ^{15}NO does not occur in a frozen matrix; rather, geminate recombination of the original isotope of ^{14}NO dominates the process. In contrast, photolysis of the "re-equilibrated" sample in solution at 5 °C does yield an altered hyperfine splitting pattern (Figure 7C). This hyperfine splitting pattern is indicative of ^{15}NO and ^{14}NO competitive binding, and thus indicates photodissociation of ^{14}NO followed by rebinding of either ^{15}NO or ^{14}NO from solution. The observation that the equilibration of ^{14}NO and ^{15}NO does not occur in the dark at 5 °C suggests that the Fe^{2+}—NO bond is very stable. This probably accounts for the apparent failure of the preformed E^r·NO complex to equilibrate with CN^- or substrate in solution.

DISCUSSION

We have previously shown that the chemically reduced iron ($3d^6$) of 3,4-PCD can bind NO to form an EPR-active complex (Orville & Lipscomb, 1993). In the absence of other strong ligands, this complex yields a $\{Fe^{2+}\cdot NO\}^7$ $S = {}^3/_2$ spin system, where the superscript 7 denotes the number of valence electrons in the system. The $S = {}^3/_2$ spin is thought to derive from the antiferromagnetic coupling of a [($3d^5$, $S = {}^5/_2$) Fe^{3+}—NO^- ($S = 1$)] electronic system (Zhang et al., 1992; Brown et al., 1995). We show here that the binding of two strong CN^- ligands in addition to NO yields a $S = {}^1/_2$ system unlike any previously described for non-heme iron proteins. Moreover, the exceptionally well-resolved hyperfine structure apparent in the EPR spectra of this complex allows identification of at least four of the iron ligands and unequivocally shows that at least three exogenous ligands can simultaneously coordinate the iron. We have also shown that the interaction of E^r with CN^- and NO is dependent upon the order in which they are presented to the enzyme as well as the incubation time. Analysis of these EPR spectra yields insights into both the structure of the active site and the iron coordination of 3,4-PCD. The bearing of these findings on the structure and mechanism of 3,4-PCD is discussed in the following sections.

Similarity to Ferrous Heme·NO Complexes. Low-spin species exhibiting hyperfine splitting of the type shown in Figures 2 and 3 are commonly observed for nitrosyl complexes of ferrous heme proteins and model complexes (Kon & Katoaka, 1969; Yonetani et al., 1972; Wayland & Olson, 1974; Sugiura, 1980; Stevens & Chan, 1981; LoBrutto et al., 1983). The integer spin of the ferrous heme is converted to a $S = {}^1/_2$, $\{Fe^{2+}\cdot NO\}^7$ electronic system through interaction with the unpaired spin of NO. In these systems, distribution of spin density among the π bonding iron d_{xz} and d_{yz} orbitals, the σ bonding orbital, the bonding and antibonding π^* orbitals of NO, and the nitrogen 2s orbital of NO determines the symmetry of the observed EPR spectrum as well as the magnitude and thus the resolution of the nuclear hyperfine coupling (LoBrutto et al., 1983; Utterback et al., 1983). Crystal structures of heme protein·NO and metalloporphyrin·NO complexes show that the NO molecule forms a short bond along the physical axis approximately normal to the heme plane (Edwards & Poulos, 1990; Edwards et al., 1988; Deatherage & Moffat, 1979; Scheidt & Frisse, 1975; Piciulo et al., 1974). The bonding interaction therefore appears to be due to an overlap of the d_z2 orbital of the iron and a bonding π^* orbital of NO (Utterback et al., 1983). Consequently, the g-tensor and nuclear hyperfine interaction tensors are closely aligned, and the largest component of the nuclear hyperfine coupling field of the nitrosyl nitrogen appears along g_z (≈2.00). However, the distribution of spin density in the complex is also proposed to be highly sensitive to the coordination geometry and Fe^{2+}—NO bond distance (Waleh et al., 1989). Indeed, crystal structures of several metalloporphyrin·NO complexes show a nonlinear Fe^{2+}—N═O bond angle (∼140−170°) and significant axial distortion due to the short, strong Fe^{2+}—NO bond. In many heme protein systems, an axial histidine ligand *trans* to the NO ligand along the principal g- and hyperfine axes yields coupling due to the transfer of spin along the π^* orbital of NO and the d_z2 orbital of the iron, causing g_z to appear as a triplet of triplets for the ^{14}NO complex and as a doublet of triplets for the ^{15}NO complex [see, for example, Yonetani et al. (1972)].

Clearly, the spectral line shape and the magnitude of the hyperfine coupling constants of the heme·NO complexes are very similar to those we report here for the $E^r\cdot(CN)_{\geq 2}\cdot NO$ complex (Table 1). This implies a heme-like, octahedral metal coordination sphere and the presence of a His ligand *trans* to the NO binding site in the $E^r\cdot(CN)_{\geq 2}\cdot NO$ complex. The octahedral symmetry is consistent with the crystal structures of several exogenous ligand complexes of the ferric enzyme (Orville et al., 1997a,b). Ligation of NO opposite a His ligand is also reasonable because two of the three sites

that can be occupied by exogenous ligands in ferric 3,4-PCD are opposite His. The highly resolved hyperfine coupling from ^{13}CN, [^{14}N]His, and ^{14}NO or ^{15}NO observed in all three resonances of the EPR spectrum strongly suggests that the principle hyperfine and *g*-tensors are closely aligned in this non-heme, low-spin complex, as is the case for most heme·NO complexes.

Low-Spin Non-Heme Iron Proteins and Model Chelate Complexes. In most of the relatively few instances of low-spin iron in non-heme metalloproteins, the iron is high-spin ferric or ferrous in the resting enzyme [see Howard and Rees (1991)], and the conversion to the low-spin state occurs as the result of strong ligand binding.[7] Our study of CN^- binding to high-spin ($S = 5/2$) ferric 3,4-PCD provides an excellent example (Orville & Lipscomb, 1989). In this case, CN^- binds to the initially high-spin ferric ion to yield a new high-spin intermediate complex. Then one or two additional CN^- molecules bind, resulting in a conversion to the low-spin $S = {}^1/_2$ state ($g = 2.43, 2.21, 1.89$). In both the high-spin intermediate and the final low-spin complex, superhyperfine interaction from $^{13}CN^-$ is observed as broadening of the EPR spectrum relative to the $^{12}CN^-$ complexes. As another example, the ferric ion within the C-terminal lobe of transferrin has also been shown to bind CN^- (Swope et al., 1988) to give a low-spin species ($g = 2.34, 2.15, 1.92$) similar to the oxidized 3,4-PCD·$(CN)_{2-3}$ complex. The kinetics of the binding reaction suggest that three CN^- molecules bind to the iron. Hyperfine coupling from $^{13}CN^-$ was explored further by ENDOR spectroscopy. Those results showed that only the $^{13}CN^-$ molecule along the g_{xx} axis of the *g*-tensor exhibits hyperfine coupling (Snetsinger et al., 1990). Comparison with the structure of lactoferrin (*e.g.*, Baker et al., 1996) and ovotransferrin (Kurokawa et al., 1995) predicts that one of the $^{13}CN^-$ binds *trans* to a His whereas the other two $^{13}CN^-$ bind opposite Tyr ligands. It is likely that the coupled $^{13}CN^-$ is bound in the unique site opposite His, whereas the other two $^{13}CN^-$ are not coupled due to weakening of their bonds to the iron by *trans* influences of the negative tyrosinate ligands. Similar *trans* ligand influences are invoked below to account for the decreased coupling from one cyanide in the E^r·$(CN)_{\geq 2}$·NO spectra.

Examples of low-spin conversions for ferrous ion containing protein complexes are even more rare. The non-heme Fe^{2+}−quinone complex at the terminal electron acceptor site in photosystem II (PS-II) has been shown to bind NO and CN^-, but not both simultaneously (Diner & Petrouleas, 1990; Petrouleas & Diner, 1990; Koulougliotis et al., 1993). The binding of excess CN^- causes conversion to a low-spin ($S = 0$) state, but NO apparently does not bind to this form (Sanakis et al., 1994). Indeed, we are unaware of any non-heme biological precedent for the $\{Fe^{2+}\cdot NO\}^7$, $S = {}^1/_2$ E^r·$(CN)_{\geq 2}$·NO complex described here which may indicate that the availability of multiple ligand sites for exogenous ligands is also relatively rare.

Perhaps, the best non-heme chelate complex for the E^r·$(CN)_{\geq 2}$·NO complex is iron bleomycin (Fe^{2+}·BLM) which binds CN^- or NO to yield low-spin complexes (Sugiura & Ishizu, 1979; Suguira, 1980). However, there is no evidence that BLM can bind more than one exogenous ligand simultaneously. The Fe^{2+}·BLM·NO adduct gives an $S = {}^1/_2$ EPR spectrum ($g = 2.041, 2.008, 1.976$) similar to that of the E^r·$(CN)_{\geq 2}$·NO complex and ferrous heme·NO complexes. However, the Fe^{2+}·BLM·NO complex exhibits an EPR spectrum with only a three-line hyperfine pattern (^{14}NO, $A = 23.6$ G). This nuclear hyperfine splitting is consistent with significant electron density on the nitrosyl ^{14}N atom in the Fe^{2+}·BLM·NO complex. No additional splitting from a *trans* nitrogen ligand is observed, suggesting either that the coupling is weak or that such a ligand is not present when NO is bound.

Iron Ligands in the E^r·$(CN)_{\geq 2}$·NO Complex. Four of the iron ligands in the E^r·$(CN)_{\geq 2}$·NO complex, two CN^-, NO, and histidine, are directly revealed by analysis of the hyperfine splitting patterns presented here. The *trans* orientations of the NO and the histidine are strongly suggested by the magnitude of the coupling constants for both NO and [^{14}N]His which are essentially the same as those observed in ferrous heme−nitrosyl complexes that contain an axial His ligand. The presence and relative orientation of the second potential histidine ligand cannot be definitively stated based on these spectroscopic data because we were unable to resolve coupling in g_z from a second ^{14}N ligand. One interpretation of this is that the second His is displaced when NO or cyanide binds. However, several X-ray crystal structures of oxidized 3,4-PCD reveal that, due to tight packing around both histidines residues, they remain coordinated to the iron in all ligand complexes examined to date (Orville et al., 1997a,b). A more likely possibility is that the nearly orthogonal alignment of the two His ligands revealed by the crystal structure of the ferric enzyme (Ohlendorf et al., 1994) directs the coupling of the second His primarily into g_x and g_y. Accordingly, the simulations of the EPR line shapes for the g_x and g_y resonances indicate a strongly coupling $I = 1$ nucleus. Although the data do not distinguish whether this coupling derives from the second His or isotropic hyperfine coupling by His *trans* to the NO, the apparent alignment of the *g*-tensor and the hyperfine coupling tensor in the E^r·$(CN)_{\geq 2}$·NO complex (see above) suggests that the coupling of this His will be anisotropic. Thus, it seems likely that the presence of the second His ligand is also revealed by the spectra reported here. The analysis of the data also strongly implies that two cyanides can coordinate simultaneously to the iron and that they exhibit similar, but distinct, coupling constants. This observation seems quite feasible based on the known crystal structures as described below.

Unifying Molecular Models for the Iron−Ligand Complexes. Atomic models for the different complexes of this report that are consistent with the order-dependent binding, numerical simulations of the EPR line shape, and the related crystal structures of oxidized 3,4-PCD are shown in Figure 8. Several of the aspects of these models are based on the principle that the neutral charge of the 3,4-PCD metal center will tend to be maintained by ligand exchange. This, in turn, is based on the observation that all 15 ferric complexes of 3,4-PCD that have been structurally characterized have a charge neutral metal center (Ohlendorf et al., 1994; Orville et al., 1997a,b). In the case of the Fe^{2+} form of 3,4-PCD, the metal has one less positive charge, and thus should preferentially bind one less negatively charged ligand to maintain neutrality. This suggests either that one of the two tyrosinate iron ligands is dissociated upon reduction or, more probably, that the solvent ligand is bound as neutral water.

[7] The exception to the rule is the non-heme iron center in nitrile hydratase which is in the low-spin state as isolated (Sugiura, 1987). Recent spectroscopic studies suggest an octahedral coordination sphere comprised of three His ligands, two *cis* Cys ligands, and an exogenous solvent molecule (Scarrow et al., 1996; Brennan et al., 1996).

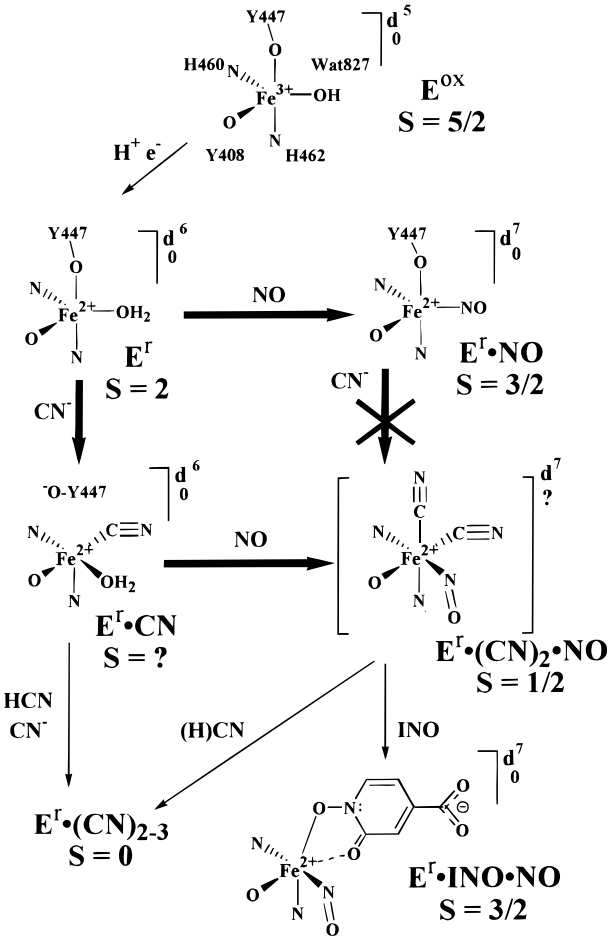

FIGURE 8: Models for the iron ligand sets that are consistent with all the experimental observations (see text for description). The total valence electron count is indicated by the superscripted d, whereas the "effective" charge of the iron complex is indicated by the subscript for each model. For example, in the uncomplexed Fe^{3+} enzyme (E^{ox}), there are five d orbital electrons (d^5), but the net charge of the metal is zero due to the three negative ligands. Because the protonation states of the cyanide and NO ligands are unknown, the overall charge of the metal centers may differ from that shown in this model However, all well-characterized states of 3,4-PCD and its complexes are neutral.

We propose that the binding of the strong anionic ligand CN^- in the equatorial site opposite Tyr408 initiates the conformational change involving the dissociation of Tyr447 to its alternate binding location so that charge neutrality of the metal is maintained. In the ferric enzyme, this conformational change also shifts the iron coordination to octahedral and creates two open coordination sites, one *trans* to each of the histidine ligands. One of these sites is adjacent to the putative O_2 binding cavity in the active site. In the oxidized 3,4-PCD•INO•CN complex, structural studies have shown that CN^- binds in this site in an unfavorable bent configuration. We propose that when NO binds to the E^r•-CN complex, it will bind strongly in this site because NO readily binds to Fe^{2+}, often with a bent configuration. This would place the NO opposite His460 (Figure 8) and account for the strongly coupled $I = 1$ ligand revealed by the superhyperfine splitting pattern of the EPR spectrum. Once bound in this protected site, the NO does not appear to readily dissociate. In contrast, the CN^- is bound in the main solvent-accessible substrate binding channel where it could readily dissociate. Moreover, the second site that is proposed to be opened as a result of CN^- binding is normally occupied by an anion (either tyrosinate or catecholate oxygen) and thus may bind the second CN^- revealed by the spectroscopic data (Figure 8). The subsequent binding of INO would be expected to displace both of the CN^- molecules because these are the sites that INO occupies in the ferric enzyme complex (Orville et al., 1997b). Since INO is known to bind in the ketonized configuration to 3,4-PCD, it would provide only one anionic ligand for the iron as required to maintain charge neutrality.[8] If both cyanides bind as anions in the E^r•$(CN)_{\geq 2}$•NO complex, it would have a charge of -1, violating the charge neutrality proposal. It is possible that cyanide is such a strong ligand that the enzyme active site environment cannot prevent this from happening. Alternatively, one of the two cyanides may be protonated, which is one way to account for the observed difference in coupling constant. Another possibility is that an electron from the Fe^{2+} is transferred to the NO, leading to an Fe^{3+} center that could accommodate an additional negative charge, as suggested by spectroscopic studies (Zhang et al., 1992). In this case, the NO would be NO^-, which would leave a net negative charge on the iron. However, the NO may also be protonated by a solvent molecule, which is revealed by the crystal structure of the oxidized enzyme in the small molecule binding pocket where we propose NO binds. Prolonged incubation of the E^r•$(CN)_{\geq 2}$•NO complex results in an EPR-silent, $S = 0$ species, suggesting that it is also possible that three or more exogenous ligand sites can be occupied simultaneously by cyanide. Again, the charge of this complex would not be neutral if all of the cyanides bind as anions, and there are no experimental data available to evaluate their ionization state.

According to the model presented in Figure 8, the binding of NO before CN^- would occur in the equatorial plane in the site proposed above for initial cyanide binding (the only site available prior to the conformational change), resulting in the displacement of the presumably neutral solvent by another neutral ligand (NO•). In addition, the transfer of electron density to the NO molecule produces ferric character on the iron. Consequently, there would be no driving force for the release of the axial Tyr447 so that neither of the potential two new sites in the iron coordination would be created. If this iron−NO bond is very stable, its formation would exclude all other ligands, as observed.

The model is also consistent with previous observations for complexes in which substrate or substrate analogs bind simultaneously with NO (Orville & Lipscomb, 1993). For the complex of ferric 3,4-PCD with monohydroxybenzoate inhibitors, the crystal structures show that the axial Tyr is not dissociated. On the basis of maintaining charge neutrality, this is the expected result because an anionic solvent ligand (Wat827) is displaced or protonated. However, in the reduced enzyme under the models proposed in Figure 8, these same inhibitors should force release of the axial Tyr because a neutral water ligand is replaced by an anion. Consequently, they should show order-dependent formation of the nitrosyl complex, and this is what was observed (Orville & Lipscomb, 1993). As another test, when sub-

[8] It is interesting to note that the difference between the INO and PCA complexes with the ferric enzyme is that the INO complex has a solvent in the putative O_2 binding site whereas this site is empty in the PCA complex (Orville et al., 1997b). This may be due to the fact that PCA appears to bind as a dianion whereas INO binds as a ketonized tautomer which can provide only one negative charge to the iron. Accordingly, the extra solvent in the INO complex may be OH^- to maintain charge neutrality.

strates bind to the reduced enzyme, our model predicts that only one of the two phenolic groups should ionize in order to maintain a neutral metal center. Accordingly, ^{17}O hyperfine broadening was observed only from the C4−O^- in the enzyme−nitrosyl complex with labeled PCA, suggesting that the C3−O(H) does not bind or is bound in the protonated form which would result in weak coupling (Orville & Lipscomb, 1993). Recently, we have investigated catechol binding to the Fe^{2+}-containing extradiol dioxygenase catechol 2,3-dioxygenase (Shu et al., 1995) using X-ray absorption spectroscopy. It was found that both in the enzyme and in a model Fe^{2+}−chelate complex, the catechol was bound asymmetrically, despite the absence of strongly electron-donating *trans* ligands, suggesting that only one of the two substrate phenol groups is ionized. This would also maintain a neutral metal center in the extradiol dioxygenase enzyme.

In the model illustrated in Figure 8, the CN^- molecule bound *trans* to $His462^{N\epsilon 2}$ would form a strong, linear Fe−C≡N bond presumably capable of effective ^{13}C hyperfine coupling with the electronic spin of the Fe^{2+}·NO system. The crystal structure of the 3,4-PCD·PCA complex shows that there would be adequate room in the space vacated by the axial Tyr447 to accommodate a linear Fe−C≡N bond. However, the CN^- bound *trans* to Tyr408 should form a somewhat weaker bond because of the *trans* influence of the tyrosinate anion The CN^- bound in this position would probably also form a hydrogen bond with Arg457 similar to substrate ligands bound in this iron ligand site (Orville et al., 1997b). This would stabilize CN^- binding in this position, but further weaken the Fe−CN bond. As a result, it is reasonable that the hyperfine coupling from $^{13}CN^-$ bound opposite Tyr408 would be weaker, possibly accounting for the small difference in hyperfine coupling constants observed for the two cyanides.

Although the model presented in Figure 8 seems reasonable based on the available structural and spectroscopic data, it is meant only to describe the simplest case and other, more complex, possibilities cannot be eliminated. For example, a simple permutation of this model could be envisioned in which NO binds opposite His462, but this coordination site for NO does not seem to satisfy the necessity of facile ligand exchange of CN^- with subsequently added INO which would presumably compete for the binding site opposite His462 as it does in the ferric enzyme. It is also difficult to eliminate explanations based on fortuitous alignments of the electronic and physical structures. Further study utilizing angle-sensitive techniques such as ENDOR or single-crystal EPR will be necessary to pursue these possibilities.

Photodissociation of the E^r·$(CN)_{\geq 2}$·NO Complex. We have demonstrated here that photolyzing the Fe^{2+}−NO bond in the E^r·$(CN)_{\geq 2}$·^{14}NO complex in solution allows exchange with ^{15}NO. In a complementary previous study (Orville & Lipscomb, 1993), we showed that NO could be photolyzed from the E^r·NO complex to allow PCA from solution to bind before the NO rebinding, thereby overcoming the order dependence of complex formation in that system. In the context of the model presented in Figure 8, we propose that in this case the NO is photodissociated from a site opposite Tyr408 and rebinds in the putative O_2 binding site opposite His460 that is created as a result of PCA binding.

Both of our studies of NO photodissociation from reduced 3,4-PCD complexes are consistent with NO migrating far enough away from its binding site to fully equilibrate with the bulk solution when the experiment is conducted above 0 °C, although this is only demonstrated directly in the current study. In contrast, at low temperatures, both studies suggest that NO does not leave the vicinity of its binding site, and molecules from the surrounding matrix do not bind to the enzyme following NO photodissociation. In these cases, the rebinding appears to be a geminate process in which the same molecule of NO that is photolyzed rebinds after the light is extinguished. A similar process has been studied in detail for photolysis of CO from myoglobin (Austin et al., 1975). For that case, the crystal structures of the photodissociated intermediate at 20 K or 40 K (Schlichting et al., 1994; Teng et al., 1994) show that the CO does not move very far from the heme iron (<2 Å) at low temperature due to structural restraints around the CO binding cavity. Therefore, the geminate rebinding process in photolyzed myoglobin·CO always includes a very fast rebinding phase at temperatures above 80 K as dictated by the immediate active site structure. Similar considerations should also apply to the active site environment around the putative O_2 cavity in 3,4-PCD. Unlike myoglobin, 3,4-PCD can bind substrates and inhibitors in addition to NO, so one might expect structural changes caused by the binding of these molecules or, indeed, the physical presence of these molecules themselves to affect the structure of the active site sampled by a photodissociated NO. According to the theories developed for geminate CO rebinding, such changes in the active site structure would affect the rebinding kinetics, which we have found to be the case. In the absence of substrates or CN^-, NO photodissociates nearly completely and rebinds slowly at 4 K, suggesting that NO is free to move relatively far from the iron and sample a large number of environments so that the kinetics of rebinding represent many processes with different rates. In contrast, when a large molecule like PCA is in the active site, the extent of dissociation is much less at the same light intensity, and the rebinding process occurs as an extremely fast phase followed by effectively no further rebinding at 4 K. This was interpreted as a binary process in which the dissociated NO either stays in a constricted space near the iron or moves past the substrate (Orville & Lipscomb, 1993). In the former location, it rebinds rapidly, but in the latter, it cannot rebind at all until the temperature is raised to provide the activation energy to surmount the barrier presented by the substrate. Photodissociation of the E^r·$(CN)_{\geq 2}$·NO complex appears to represent a case in between the E^r·NO and E^r·PCA·NO cases, as might be expected from the lesser bulk of CN^- and our proposal that it can occupy two binding positions. The extent of photodissociation is about halfway between those observed for the E^r·NO and E^r·PCA·NO cases, but the rebinding process resembles that of the photodissociated E^r·NO complex. Thus, CN^- clearly affects NO dissociation and rebinding rates, but NO still appears to be able to sample much more of the active site than when PCA is present. This seems fully consistent with the model presented in Figure 8.

Implications for the Reaction Mechanism. The current mechanistic hypothesis (Orville et al., 1997b) for 3,4-PCD stresses. (i) the importance of the use of multiple ligand sites of the iron to carry out catalysis, (ii) the dynamic change in the number and availability of these sites during turnover to enforce specificity, and (iii) the influence of ligands *trans* to these sites to create the asymmetry that is important to specific bond-breaking reactions. The current study probes

these effects through the use of simultaneous binding of ligands to multiple sites in the iron coordination to yield an EPR-active state that is sensitive to many aspects of the complex that is formed. Clearly, multiple ligand sites are available to exogenous ligands, but access to these sites is controlled by the nature of the ligand that binds first. If the ligand that binds first is an anion, like the bound form of substrates, more sites become available for other ligands that participate in the catalyzed reaction as is proposed in the molecular mechanism. Finally, small differences in the coupling constants for the two bound cyanide ligands may reveal the effects of the *trans* ligands in the iron coordination sphere. Although 3,4-PCD provides an excellent example of these different roles of a metal and its ligands in a biological system, it is likely that these aspects of metal-based catalysis are also generally applicable to the broad family of metalloenzymes.

ACKNOWLEDGMENT

We thank Dr. Eckard Münck and Dr. Brian G. Fox for collection and analysis of the Mössbauer data and for many insightful discussions. We thank K. Dolbeare for measurement of the mixed cyanide isotope spectra and acknowledge a reviewer of this paper for pointing out an alternative coupling scheme for ^{13}CN. We also thank J. Dege and D. Dyer for assistance in preparation of the enzymes.

REFERENCES

Aasa, R., & Vånngärd, T. (1975) *J. Magn. Reson. 19*, 308−315.
Arciero, D. M., Lipscomb, J. D., Huynh, B. H., Kent, T. A., & Münck, E. (1983) *J. Biol. Chem. 258*, 14981−14991.
Arciero, D. M., Orville, A. M., & Lipscomb, J. D. (1985) *J. Biol. Chem. 260*, 14035−14044.
Austin, R. H., Beeson, K. W., Eisenstein, L., Frauenfelder, H., & Gunsalus, I. C. (1975) *Biochemistry 14*, 5355−5373.
Baker, H. M., Anderson, B. F., Brodie, A. M., Shongwe, M. S., Smith, C. A., & Baker, E. N. (1996) *Biochemistry 35*, 9007−9013.
Bolton, J. R. (1972) in *Biological Applications of Electron Spin Resonance* (Schwartz, H. M., Bolton, J. R., & Borg, D. C., Eds.) p 61, Wiley & Sons Inc., New York.
Brennan, B. A., Cummings, J. G., Chase, D. B., Turner, I. M., Jr., & Nelson, M. J. (1996) *Biochemistry 35*, 10068−10077.
Brown, C. A., Pavlosky, M. A., Westre, T. E., Zhang, Y., Hedman, B., Hodgson, K. O., & Solomon, E. I. (1995) *J. Am. Chem. Soc. 117*, 715−732.
Deatherage, J. F., & Moffat, K. (1979) *J. Mol. Biol. 134*, 401−417.
Diner, B. A., & Petrouleas, V. (1990) *Biochim. Biophys. Acta 1015*, 141−149.
Edwards, S. L., & Poulos, T. L. (1990) *J. Biol. Chem. 265*, 2588−2595.
Edwards, S. L., Kraut, J., & Poulos, T. L. (1988) *Biochemistry 27*, 8074−8081.
Felton, R. H., Gordon, S. L., Sowell, A. L., & May, S. W. (1984) *Biochemistry 23*, 3955−3959.
Ferrin, T. E., Huang, C. C., Jarvis, L. E., & Langridge, R. (1988) *J. Mol. Graphics 6*, 13−27.
Howard, J. B., & Rees, D. C. (1991) *Adv. Protein Chem. 42*, 199−280.
Kon, H., & Katoaka, N. (1969) *Biochemistry 8*, 4757−4762.
Koulougliotis, D., Kostopoulos, T., Petrouleas, V., & Diner, B. A. (1993) *Biochim. Biophys. Acta 1141*, 275−282.
Kurokawa, H., Mikami, B., & Hirose, M. (1995) *J. Mol. Biol. 254*, 196−207.
Lipscomb, J. D., & Orville, A. M. (1992) *Met. Ions Biol. Syst. 28*, 243−298.
LoBrutto, R., Wei, Y.-H., Mascarenhas, R., Scholes, C. P., & King, T. E. (1983) *J. Biol. Chem. 258*, 7437−7448.
Ohlendorf, D. H., Lipscomb, J. D., & Weber, P. C. (1988) *Nature 336*, 403−405.
Ohlendorf, D. H., Orville, A. M., & Lipscomb, J. D. (1994) *J. Mol. Biol. 244*, 586−608.
Orville, A. M., & Lipscomb, J. D. (1989) *J. Biol. Chem. 264*, 8791−8801.
Orville, A. M., & Lipscomb, J. D. (1993) *J. Biol. Chem. 268*, 8596−8607.
Orville, A. M., Chen, V. C., Kriauciunas, A., Harpel, M. R., Fox, B. G., Münck, E., & Lipscomb, J. D. (1992) *Biochemistry 31*, 4602−4612.
Orville, A. M., Elango, N., Lipscomb, J. D., & Ohlendorf, D. H. (1997a) *Biochemistry 36*, 10039−10051.
Orville, A. M., Lipscomb, J. D., & Ohlendorf, D. H. (1997b) *Biochemistry 36*, 10052−10066.
Petrouleas, V., & Diner, B. A. (1990) *Biochim. Biophys. Acta 1015*, 131−140.
Piciulo, P. L., Rupprecht, G., & Scheidt, W. R. (1974) *J. Am. Chem. Soc. 96*, 5293−5295.
Que, L., Jr. (1989) in *Iron Carriers and Iron Proteins* (Loehr, T. M., Ed.) pp 467−524, VCH, New York.
Que, L., Jr., & Ho, R. Y. N. (1996) *Chem. Rev. 96*, 2607−2624.
Que, L., Jr., Lipscomb, J. D., Zimmermann, R., Münck, E., Orme-Johnson, N. R., & Orme-Johnson, W. H. (1976) *Biochim. Biophys. Acta 452*, 320−334.
Sanakis, Y., Petrouleas, V., & Diner, B. A. (1994) *Biochemistry 33*, 9922−9928.
Scarrow, R. C., Brennan, B. A., Cummings, J. G., Jin, H., Duong, D. J., Kindt, J. T., & Nelson, M. J. (1996) *Biochemistry 35*, 10078−10088.
Scheidt, W. R., & Frisse, M. E. (1975) *J. Am. Chem. Soc. 97*, 17−21.
Schlichting, I., Berendzen, J., Phillips, G. N., Jr., & Sweet, R. M. (1994) *Nature 371*, 808−812.
Snetsinger, P. A., Chasteen, N. D., & van Willigen, H. (1990) *J. Am. Chem. Soc. 112*, 8155−8160.
Stevens, T. H., & Chan, S. I. (1981) *J. Biol. Chem. 256*, 1069−1071.
Sugiura, Y. (1980) *J. Am. Chem. Soc. 102*, 5208−5215.
Sugiura, Y., & Ishizu, K. (1979) *J. Inorg. Biochem. 11*, 171−180.
Sugiura, Y., Kuwahara, J., Nagasawa, T., & Yamada, H. (1987) *J. Am. Chem. Soc. 109*, 5848−5850.
Swope, S. K., Chasteen, N. D., Weber, K. E., & Harris, D. C. (1988) *J. Am. Chem. Soc. 110*, 3835−3840.
Teng, T.-Y., Šrajer, V., & Moffat, K. (1994) *Struct. Biol. 1*, 701−705.
True, A. E., Orville, A. M., Pearce, L. L., Lipscomb, J. D., & Que, L., Jr. (1990) *Biochemistry 29*, 10847−10854.
Utterback, S. G., Doetschman, D. C., Szumowski, J., & Rizos, A. K. (1983) *J. Chem. Phys. 78*, 5874−5880.
Waleh, A., Ho, N., Chantranupong, L., & Loew, G. H. (1989) *J. Am. Chem. Soc. 111*, 2767−2772.
Wayland, B. B., & Olson, L. W. (1974) *J. Am. Chem. Soc. 96*, 6037−6041.
Whittaker, J. W., & Lipscomb, J. D. (1984a) *J. Biol. Chem. 259*, 4487−4495.
Whittaker, J. W., & Lipscomb, J. D. (1984b) *J. Biol. Chem. 259*, 4476−4486.
Whittaker, J. W., Lipscomb, J. D., Kent, T. A., & Münck, E. (1984) *J. Biol. Chem. 259*, 4466−4475.
Whittaker, J. W., Orville, A. M., & Lipscomb, J. D. (1990) *Methods Enzymol. 188*, 82−88.
Yonetani, T., Yamamoto, H., Erman, J. E., Leigh, J. S., Jr., & Reed, G. H. (1972) *J. Biol. Chem. 247*, 2447−2455
Zhang, Y., Pavlosky, M. A., Brown, C. A., Westre, T. E., Hedman, B., Hodgson, K. O., & Solomon, E. I. (1992) *J. Am. Chem. Soc. 114*, 9189−9191.

BI970609L